

Article

Numerical Simulation of Local Climate Zone Cooling Achieved through Modification of Trees, Albedo and Green Roofs—A Case Study of Changsha, China

Yaping Chen ¹, Bohong Zheng ^{1,*} and Yinze Hu ²

¹ Architecture and Art School, Central South University, Changsha 410075, China; 171301014@csu.edu.cn

² Business School, Hunan University, Changsha 410082, China; huyinze@hnu.edu.cn

* Correspondence: zhengbohong@csu.edu.cn

Received: 25 February 2020; Accepted: 24 March 2020; Published: 1 April 2020



Abstract: By exploring the cooling potential of tree quantity, ground albedo, green roofs and their combinations in local climate zone (LCZ)-4, LCZ-5, and LCZ-6, this study focuses on the optimum cooling level that can be achieved in open residential regions in Changsha. It designs and models 39 scenarios by integrating in situ measurement and ENVI-met numerical simulation and further compares cooling effects of various combinations of the cooling factors. The results show that (1) an increased number of trees and higher albedo are more effective compared to green roofs in reducing summer potential temperatures at street level (2 m high) in three LCZs. Negative correlations are observed in the pedestrian air temperature with trees and ground albedo; (2) the effects of cooling factors vary among different LCZ classes, with the increased 60% more trees leading to lower outdoor temperatures for LCZ-4 (0.28 °C), LCZ-5 (0.39 °C), and LCZ-6 (0.54 °C), while higher albedo of asphalt surface (increased by 0.4) is more effective in LCZ-4 (reaches to 0.68 °C) 14:00, compare to LCZ-5 (0.49 °C) and LCZ-6 (0.38 °C); (3) applying combined cooling methods can provoke air temperature reduction (up to 0.96 °C), especially when higher levels of tree quantities (increased by 60%) are coupled with cool ground materials (albedo increased by 0.4). The results can contribute useful information for improving thermal environment in existing residential regions and future residential planning.

Keywords: local climate zones; ENVI-met; numerical simulation; thermal environment mitigation

1. Introduction

Rapid urbanization leads to the transformation of vegetation area, water bodies, and cultivated land into urban buildings and impervious ground. These transformations reduce the evapotranspiration of vegetation and increase the absorption of solar radiation by impervious materials, resulting in higher air and surface temperatures in urbanized city center areas than in surrounding rural regions, thus forming the urban heat island (UHI) phenomenon [1]. Extreme heat events (EHE) [2] caused by the UHI not only lead to climatological problems [3] but also have an impact on public health [4–6] and even contribute to mortality among the urban population [7–9]. Recently, urban planning strategies have gained importance when UHI mitigation and sustainable development of the cities are considered [10]. In fact, a number of studies have been conducted on how the land surface properties (vegetation, material, and buildings) contribute to the urban microclimate conditions [11–17] as well as how the optimized urban physical properties facilitate energy reduction [18–20] to maintain the comfortable urban thermal environment and make the city more livable and sustainable.

Among the many UHI mitigation strategies, greenery has been regarded as one of the valid measures to have significant cooling effects. By increasing the quantity of vegetation [21,22] or

vegetation ratio [23], applying appropriate plant layout [24–26], and choosing the right vegetation species [27,28], the urban heat load can be alleviated efficiently. The cooling effect of green space is also closely related to tree canopy coverage and size [29]. As a result, vegetation can counteract the effects of solar radiation by shadows and evaporation, trees, shrubs, and lawns that reduce regional and local temperatures [30–32].

Changes in methods used to build roofs and pavement materials are also able to produce a cooling effect [33–35]. Green roofs have been widely accepted as one of the nature-based solutions to mitigate UHI and building energy consumption [36–38], especially in the densely built-up environment where few surfaces at the ground level are available for greening [6]. The soil and vegetation layers of green roofs can reduce the short-term fluctuation of air temperature [39]. Moreover, green roofs not only save energy for buildings in summer but also help keep buildings warm in winter [19,40]. Although most of the studies have confirmed that the air temperature above the green roof is lower than that of the traditional roof [41], reducing the energy consumption for building cooling [42], few studies have explored the impact of the green roof on the air temperature at the pedestrian height.

Albedo, which indicates the fraction of shortwave radiation reflected by the surface material, is often discussed as a factor affecting the ground temperature and air temperature. An albedo of 0 means no reflecting power of a perfectly black surface, while an albedo of 100% means perfect reflection off an entirely white surface [43]. The relatively low albedo and subsequent more thermal energy storage in pavement tend to generate a more severe UHI effect [43–45], whereas the high albedo materials covering urban surfaces are able to counteract the temperature increase [46,47] and thereby mitigate the UHI [48]. Although pavement with high albedo can reduce air temperature, the value of thermal comfort index (physiological equivalent temperature, PET) may be increased by growing mean radiation temperature (MRT) due to the greater solar reflection [49,50]. To sum up, although there are many studies focusing on the cooling effect of a single factor, in reality, many cooling measures are often implemented at the same time, and the combined cooling effect of microclimate influencing factors lacks further discussions.

In addition, previous studies have shown that urban microclimate conditions are not only affected by vegetation and materials but also by physical properties of buildings (surface fraction, height, and sky view factor, etc.), which affect local climate through their modification of airflow, atmospheric heat transport, and shortwave and longwave radiation balances [51,52]. Some studies propose that strategies for optimizing greenery design with regard to the built environment and local climatic conditions can enhance thermal benefits of vegetation in urban areas [25,53]. However, research on the context-based planning and design strategies for the cooling method is scarce. Moreover, it is difficult to apply these thermal environment mitigation schemes to other cases. The application of the local climate zone (LCZ) [54] scheme can solve this dilemma. The concept of local climate zone, which was brought up by Stewart and Oke in 2012, provides a research framework for the standardization of urban spatial forms. According to the threshold range of measurable surface parameters, such as building height, building surface fraction, sky view factor, aspect ratio, impervious surface fraction, pervious surface fraction, and terrain roughness class, the LCZs can be categorized by two basic classes: built-up class and land cover class. The built-up LCZs comprise 10 classes (LCZ-1-10), which are classified by the compactness and openness of the building layout, as well as the building height, building materials, and human activities, while the land cover LCZs consist of seven classes (LCZ-A-G), which are distinguished by the surface coverage type, vegetation density, and height. LCZs are areas of uniform surface cover structure, material, and human activity [54] with corresponding thermal properties [55,56] and may range from hundreds of meters to several kilometers on the horizontal scale [57].

The advantages of applying the LCZ scheme are, on the one hand, since each LCZ class has a generally unique building height and density, as well as some predominant types of building material (concrete, masonry, metal, glass, wood, etc.) [58], the building environment of the study is predetermined in order to propose the targeted cooling strategies of the selected LCZs. On the other

hand, as the LCZ method a universally comparable approach for urban microclimatology, it can be used as a reference to the local climate areas with similar spatial forms in other cities. With the adoption of the LCZ concept, urban thermal environment studies have been put into a new experimental framework, which is to detect the characteristics of air temperature (T_a) and analyze the T_a differences of LCZ classes. Compared to the mobile temperature observations [59,60] which tend to an overview of the air temperature distribution of the LCZ map, numerical simulation of air temperature in each LCZ is more precise in microclimates at a neighborhood scale. For example, through the ENVI-met software simulation, Ariane Middel designed five compact and open LCZs to evaluate the air temperature near the ground, with the conclusion that the high-density LCZ class has a cooling effect at 15:00 [61]. Six different local climate zones (LCZs) in Vancouver, Canada, have been studied to find a heat mitigation strategy to reduce or maintain current T_{mrt} under projected climate scenarios for selected LCZs using the solar and longwave environmental irradiance geometry (SOLWEIG) model, the results of which show that increasing street tree coverage can increase the cooling effect of radiation [62]. However, the T_a simulation results of inter-LCZs are still not adequate to cover all the LCZ classes and cities under different climate conditions. Therefore, there is a need to provide further references for improving outdoor thermal comfort and future urban planning.

The overall objective of this research is not limited to the influence of a single variable on the results of the microclimate; more importantly, it studies and evaluates the influence of cooling method combinations in each open LCZ, which is instructive for the optimization of urban development programs at the neighborhood and street scales. The main problems to be solved are as follows: (1) the impact of single variables (vegetation, ground albedo, and green roof) on pedestrian air temperature in the same LCZ type; (2) under the identical LCZ condition, whether the cooling outcome of combined measures on air temperature is better than the impact of the single method; (3) whether the cooling outcome of the same measure is distinct in the different LCZ, and trying to find the optimized cooling combinations for air temperature reduction in LCZ-4 (open high-rise), LCZ-5 (open middle-rise) and LCZ-6 (open low-rise).

In this study, the air temperature of pedestrian height (2 m) in LCZ-4, LCZ-5, and LCZ-6 is simulated and analyzed by on-site measurement, as well as the numerical simulation method (ENVI-met), which has the advantage of space–time precision. Through the variable simulations, 39 scenarios including three current scenarios are examined on a typical summer day of Changsha, China (1 August 2019). The results indicate that applying combined cooling factors can maximize the cooling effect in LCZ-4-6, especially when higher levels of tree quantity are coupled with higher albedo ground material, which may also provide important insights for urban planners to improve the urban thermal environment.

2. Materials and Methods

2.1. Target Region

Changsha is the capital city of Hunan Province, which is located in the southeast of China. The regional range of Changsha is $111^{\circ}53'–114^{\circ}15'$ E and $27^{\circ}51'–28^{\circ}41'$ N. Changsha City has a subtropical monsoon humid climate, which is extremely hot in summer and cold in winter. The dominant wind is southeast in summer and northwest in winter. From late May, there are 85 days when the daily average temperature is above 30°C in summer, and 30 days when the temperature is above 35°C [63].

Three residential areas were selected as the research object in Changsha, which are an open arrangement of high-rise buildings (LCZ-4), mid-rise buildings (LCZ-5), and low-rise buildings (LCZ-6) (Figure 1). In order to avoid the interference brought by geographical location, the research objects are located in the adjacent blocks of Yuelu District of Changsha. However, the area of the three residential areas occupied are quite different, which may influence the comparison results of the three LCZs. In order to cover the same area in each LCZ, an area of 120×120 m of each residential area is defined (Figure 2), which means the areas outside the simulation domain also feature similar surface

properties to the simulated areas. The three classes contain the characteristic of open LCZs, which have an abundance of pervious land cover (low plants, scattered trees), as well as concrete, steel, stone, and glass construction materials [54]. Table 1 shows the comparison of geometric and surface cover properties' values between standard statistics and the study cases. Although three figures do not align with the surface property values of LCZ-4 and LCZ-6, the selected three sites are identified and described with the best-fit LCZ class, which is allowed in the LCZ classification [54]. In order to avoid the interference brought by geographical location, the research objects are located in the adjacent blocks of Yuelu District of Changsha.

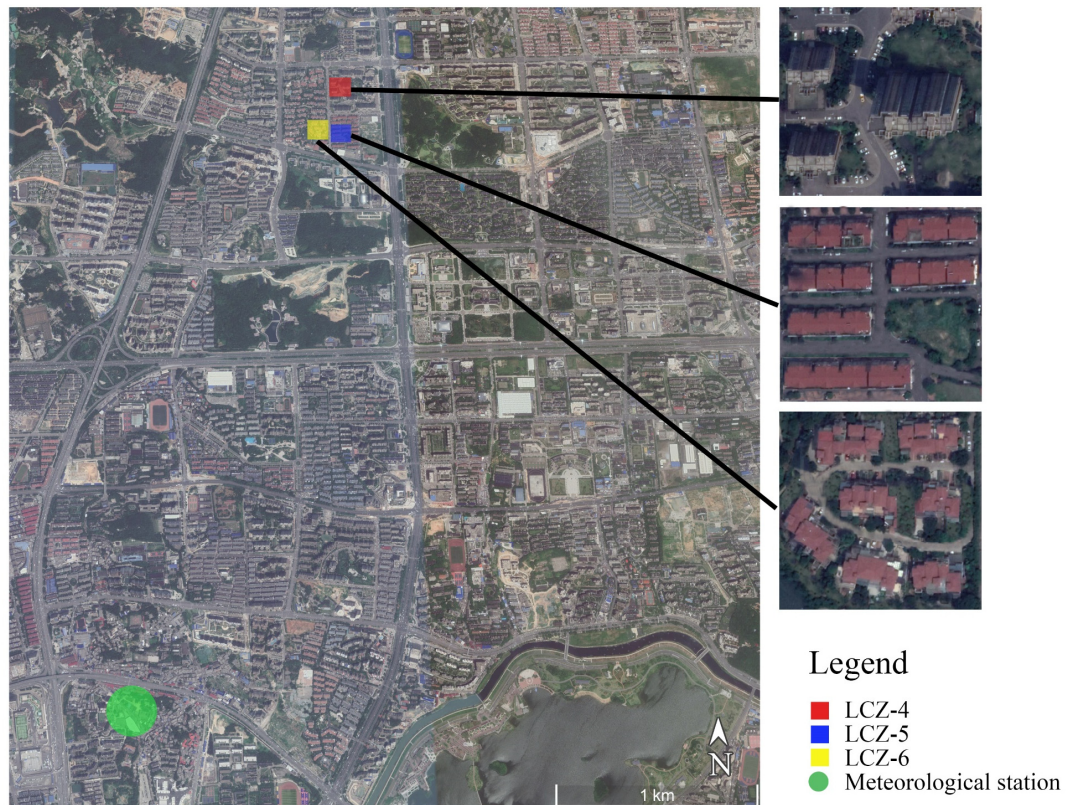


Figure 1. The location of local climate zone (LCZ)-4, LCZ-5, LCZ-6, and the Changsha meteorological station.

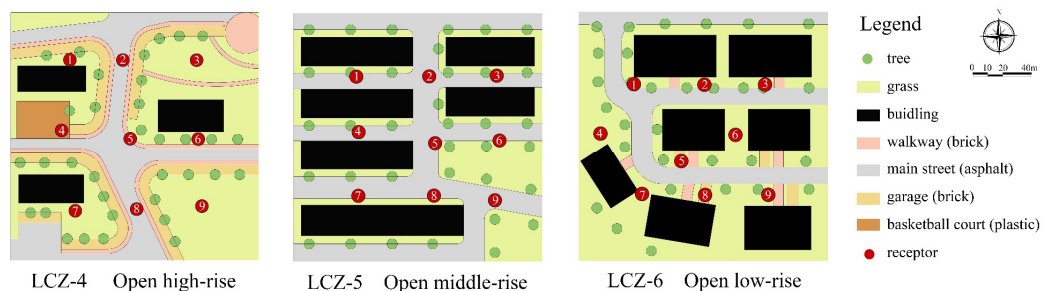


Figure 2. Baseline scenario plan of LCZ-4, LCZ-5, and LCZ-6.

To further calculate the parameters, in the center of each site, the fisheye camera was used at 2 m to calculate the sky view factor, which indicates the ratio of the amount of sky hemisphere visible from ground level to that of an unobstructed hemisphere. The aspect ratio was calculated through mean height-to-width ratio of street canyons, while the building surface fraction is the ratio of building plan area to total plan area. Additionally, the impervious surface fraction is the ratio of impervious plan area (paved, rock) to total plan area, and the pervious surface fraction refers to the ratio of pervious plan area (bare soil, vegetation, water) to total plan area.

Table 1. The comparison of geometric and surface cover properties' values between standard statistics [58] and study cases.

LCZ Class	Sky View Factor		Aspect Ratio		Building Surface Fraction		Impervious Surface Fraction		Pervious Surface Fraction		Building Height	
	standard	case	standard	case	standard	case	standard	case	standard	case	standard	case
LCZ-4 Open high-rise	0.5–0.7	0.62	0.75–1.25	1.11	20–40	11.04 ¹	30–40	50.54 ¹	30–40	30.46	>25	96
LCZ-5 Open midrise	0.5–0.8	0.51	0.3–0.75	0.44	20–40	24.58	30–50	42.09	20–40	33.91	10–25	18
LCZ-6 Open low-rise	0.6–0.9	0.68	0.3–0.75	0.36	20–40	17.70 ¹	20–50	30.59	30–60	50.41	3–10	9

¹ Values that are not consistent with the standard LCZ statistics.

2.2. Model Settings

The simulation area was 120 × 120 m, with the number of horizontal grids being 49 × 49 (horizontal resolution is 2.5 m). A nested grid was set around the site, with ground type loam, which is a buffer zone that can be created outside the core area to solve problems with the model not working reliably at and near the borders [17]. On the basis of the report of Hunan Meteorological Bureau, China, in 2019 [64], there were 22 days of high temperature from 12 July to 20 August in Changsha City, and the highest average air temperature appeared on 1 August 2019. Therefore, the simulation started at 7:00 on 1 August 2019 and ended at 7:00 on 2 August 2019 for 24 hours, with the initial temperature 33.12 °C, the wind speed 2.2 m/s, the wind direction southeast 150°, and the humidity 56.50% [63]. In the simulated models, nine receivers were arranged proximately every 30 m (Figure 2).

The full forcing function developed by ENVI-met 4.0 was used to drive the simulation with external meteorological data as boundary conditions. The data come from the Changsha meteorological station (No. 57687, location 112°.91' E, 28°.21' N), which is approximately 3.38 kilometers from the block where the three sites are located (112°.93' E, 28°.24' N) (Figure 1). The meteorological station of Changsha is one of the national surface stations that provides hourly data, including hourly observational values of such weather elements as temperature, pressure, relative humidity, moisture pressure, wind, and precipitation. Other than that, it also needs vegetation data, soil data, building data, and ground data. The plant height and crown width are estimated according to the actual measurement from the site. The leaf area density (LAD) is based on the measured values of *Cinnamomum camphora* and *Photinia rubra*. The LAD of grassland is set as the default value from ENVI-met. The thermal properties of ground materials are set according to “Code for thermal design of civil building (GB 50176-2016)” [65]. The initial soil temperature and humidity are set based on general values [66]. Table 2 lists the main input parameters of the ENVI-met simulation.

Table 2. The main input parameters of ENVI-met.

	Meteorological Data	Vegetation Data	Soil Data	Ground Material Data
Data	Meteorological data of 1 August 2019	Tree: <i>Cinnamomum camphor</i> , height = 15.00 m, crown width = 8.00 m, leaf area density = 1.80 m ² /m ³		
	Initial air temperature: 33.12 °C	Shrub: <i>Photinia rubra</i> , height = 1.00 m, leaf area density = 2.50 m ² /m ³	0–20 cm: 305 K/30%; 20–50 cm: 307 K/40%; Blow	Asphalt: grey, albedo = 0.1
	Wind velocity: 2.20 m/s	Lawn: Manila grass, height = 0.20 m, leaf area density = 0.30 m ² /m ³	50 cm: 306 K/50%	Bricks: default data
	Wind direction: southeast, 150°	Green roof: <i>Sedum emarginatum</i> Migo, height = 0.10 m, leaf area density = 0.30 m ² /m ³		
	Relative humidity: 56.50%			

The accuracy of ENVI-met was tested by the data measured at test point #5 in the open high-rise model, open middle-rise model, and open low-rise model in the summer. The air temperature was recorded by the HOBO Temperature/Humidity Data Logger (model H 08-032-08) at a height of 2 m above the ground at the #5 receiver location in each LCZ scenario (Figure 3). Since humidity is not considered in this study, the data of humidity were not recorded. The HOBO data logger has a temperature operating range of -30 to 50 °C and a resolution of 0.02 °C at 21 °C. The on-site T_a measurement was applied on 22 July 2019, which was the day after Changsha Meteorological Observatory issued the first high-temperature yellow early warning signal, in order to test the accuracy of ENVI-met under the extreme hot weather condition. Therefore, the validation measurement duration was 24 hours from 10:00 on 22 July to 10:00 on 23 July 2019, and the output data interval was set at every 6 minutes. Since the first three hours of simulation in ENVI -met is unstable, it was discarded. Thus, the simulations were from 7:00 of 22 July to 10:00 of 23 July 2019.

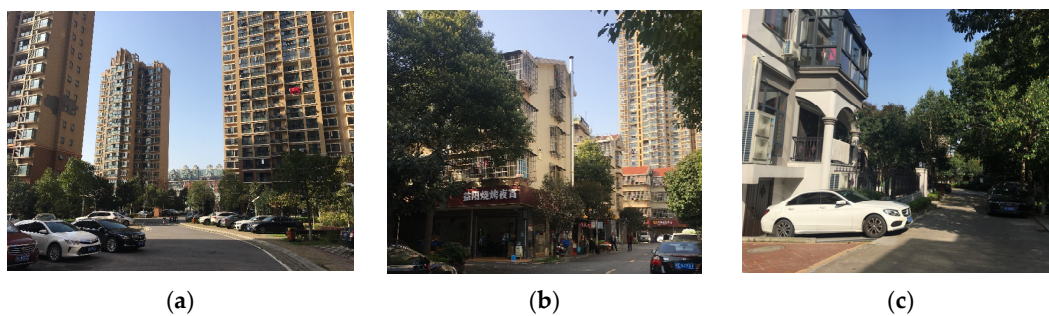


Figure 3. Real scenarios of (a) LCZ-4, (b) LCZ-5, and (c) LCZ-6.

The sensitivity of measured and simulated data was analyzed with correlation measures and difference measures. The correlation evaluation index (R^2) was used to quantify the correlation degree between the simulation value and the observation value, while the root mean square error (RMSE) evaluated the error between the two indexes. The RMSE expression is as follows,

$$RMSE = \sqrt{\frac{\sum_{i=1}^n (X_{obs,i} - X_{model,i})^2}{n}} \quad (1)$$

2.3. Model Validation

From Figure 4, the RMSE and R^2 of the two sets of data are 1.39 °C and 0.89 , respectively, in LCZ-4. For LCZ-5, the RMSE is the lowest (0.67 °C), and R^2 is 0.97 , while for LCZ-6, RMSE is 1.44 °C, and R^2 is 0.88 . Similarities were found in the three scenarios, which are, from 12:00 to 18:00, the actual air temperature is significantly underestimated in the simulation results, while from 19:00 to 2:00, the simulated temperature data are higher than the actual measurement data.

Previous studies have reported simulation errors, which could be caused by many reasons [60,67,68]. Firstly, the anthropogenic heat release is not taken into consideration [69,70], leading to underprediction of daytime T_a . Secondly, the ENVI-met simulation maintains a single wind direction for the entire simulation period, which introduces uncertainty into the model results. Overall, it can be concluded that ENVI-met simulations provide acceptable accuracy regarding outdoor air temperatures in this study.

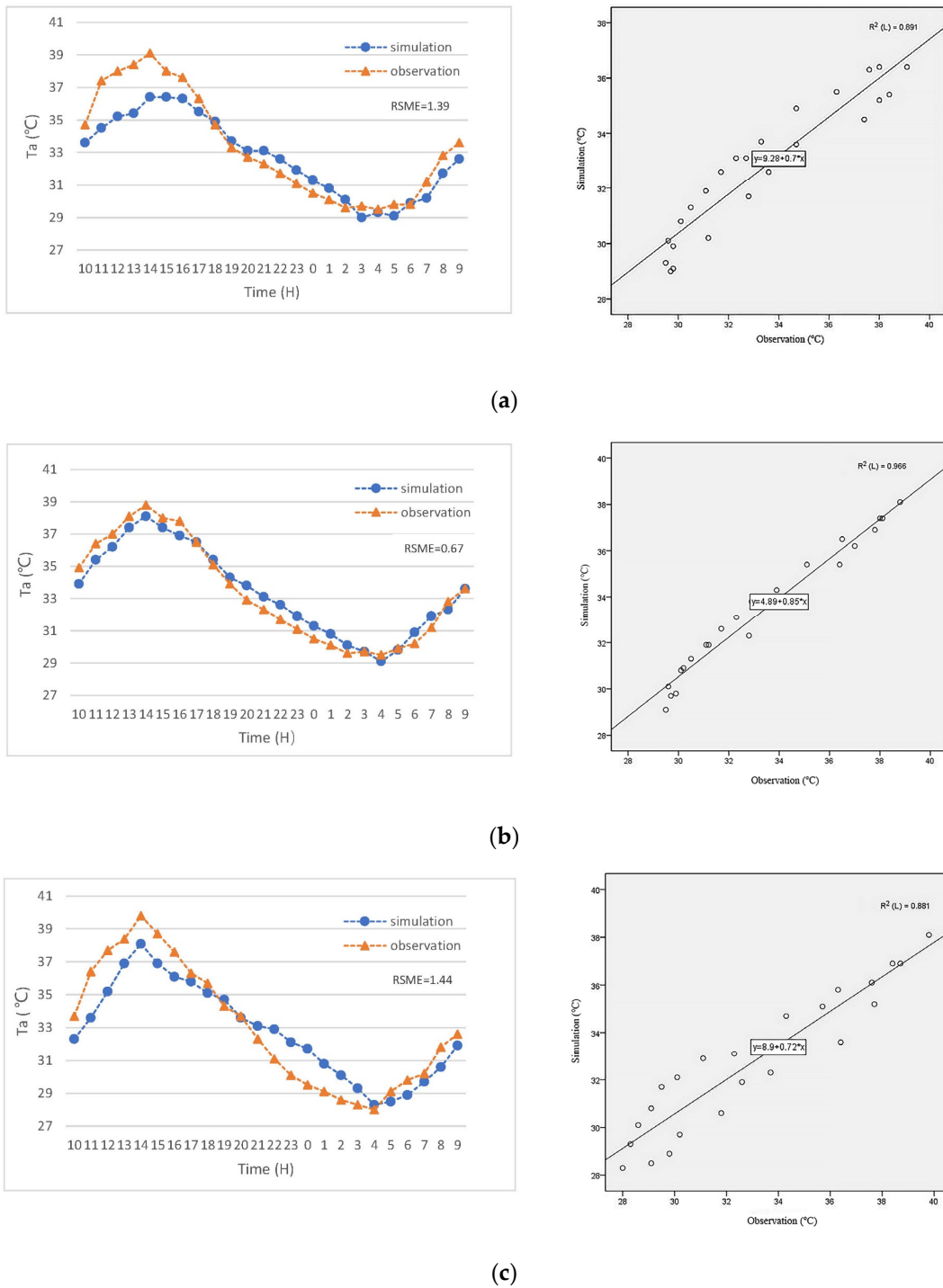


Figure 4. (a) Root mean square error (RMSE) and R^2 of simulated and observed results at point #5 in LCZ-4; (b) RMSE and R^2 of simulated and observed results at point #5 in LCZ-5; (c) RMSE and R^2 of simulated and observed results at point #5 in LCZ-6.

2.4. Vegetation and Material Variable Settings

The numerical simulations were conducted to examine the cooling potential of different modifications on urban microclimates by considering the original form of LCZ-4 (open high-rise buildings), LCZ-5 (open middle-rise buildings), and LCZ-6 (open low-rise buildings) as three Baseline scenarios. There are other 36 scenarios for this study, which are 12 cooling strategy scenarios applied for LCZ-4, LCZ-5, and LCZ-6 (Table 3).

In the outdoor thermal environment, the ability of plant types to reduce the air temperature of pedestrian height is trees > lawn > shrub [29] according to the order of cooling effect from strongest to weakest, so for the tree factor, on the basis of the Baseline scenario, the study designed and simulated the situation of adding different numbers of trees (30% and 60%) (Table 4). In Scenario A and Scenario B, trees were added along the road (Figure 5). There are two reasons for this modification: First, in order to explore how to reduce the temperature with minimum modification to the current situation, it only increases the number of trees, and thereby the existing evenly spaced trees along the road are maintained. Second, as found in the simulation of all the Baseline scenarios at 14:00, the hard paved area presents higher temperature. Therefore, the study assumes that the arrangement of trees along the road is more effective in cooling.

Table 3. Vegetation and material variable settings for each scenario.

No.	1	2	3	4	5	6
Single-variable	Adding trees 30%	Adding trees 60%	Green roof 50%	Green roof 100%	Increase albedo 0.2	Increase albedo 0.4
no.	7	8	9	10	11	12
Scenario	Scenario A+C	Scenario A+E	Scenario B+D	Scenario B+F	Scenario C+E	Scenario D+F
Double-variable	Adding trees 30% Green roof 50%	Adding trees 30% Increase albedo 0.2	Adding trees 60% Green roof 100%	Adding trees 60% Increase albedo 0.4	Green roof 50% Increase albedo 0.2	Green roof 100% Increase albedo 0.4

Table 4. Variables of each LCZ.

	Tree			Albedo			Green Roof		
	current	add	increase by	current	increase	increase to	current	add	increase by
LCZ-4 (open high-rise)	34	10 20	30% 60%	0.1	0.2 0.4	0.3 0.5	1580	790 1580	50% 100%
LCZ-5 (open middle-rise)	36	11 22	30% 60%	0.1	0.2 0.4	0.3 0.5	3450	1725 3450	50% 100%
LCZ-6 (open low-rise)	31	9 18	30% 60%	0.1	0.2 0.4	0.3 0.5	2450	1225 2450	50% 100%

A green roof typically is a vegetative layer with a growing medium over a waterproofing membrane [71]. It usually has two distinctive types, intensive and extensive. Intensive green roofs come with very high maintenance costs and heavy structural support because they employ deep growth media and high growth media for trees and shrubs [72], while extensive green roofs are cost-effective and easy to maintain, with a thin layer of vegetation and shallow soil [41]. Therefore, this study only considers the extensive green roof, which is more widely used. In this case, the *Sedum emarginatum* Migo species was considered in the green roof modelling, due to its long life cycle and great drought tolerant ability [73]. Meanwhile, the height of the soil layer and vegetation layer were both set to 0.10 m. In Scenario C, 50% roofs were replaced with green roofs, while in Scenario D, 100% roofs were covered by green roofs. The layouts are shown in Figure 6.

Replacing urban surfaces with high-albedo materials is a common strategy to mitigate UHI [74]. In this study, asphalt is the most dominant material for the main streets in the Baseline scenario, which is also the ground material taking up large space in each LCZ. The parking lot grounds in LCZ-4 and LCZ-6, as well as the walkway in LCZ-4, are made of brick, and the basketball court in LCZ-4 is plastic, which only takes up a small percentage. Therefore, the parking lot and basketball court sections remain unchanged in the variable settings (Figure 2). Since the current street is covered with asphalt, where solar radiation is absorbed due to the low albedo [50], the albedo of the asphalt pavement on the streets was increased by 0.2 and 0.4 respectively in Scenario E and Scenario F, that is, to change the value of

reflection in the database manager in ENVI-met. Although the research shows that roof surfaces and building walls can also reflect radiation [14], this is not considered in this study.

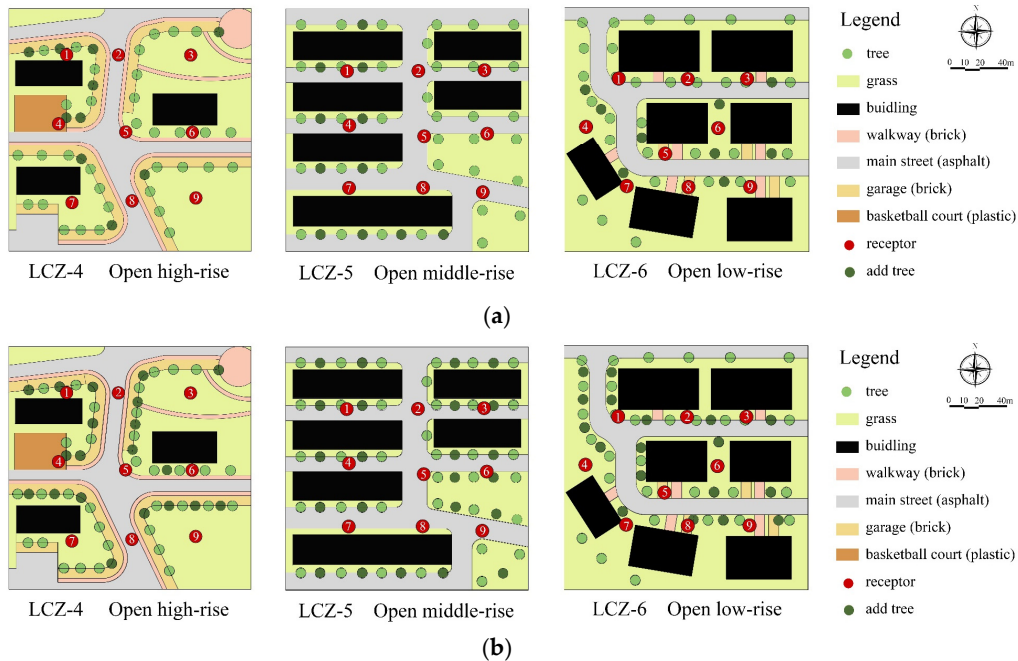


Figure 5. (a) Adding 30% tree quantity in LCZ-4, LCZ-5, and LCZ-6; (b) Adding 60% tree quantity in LCZ-4, LCZ-5, and LCZ-6.

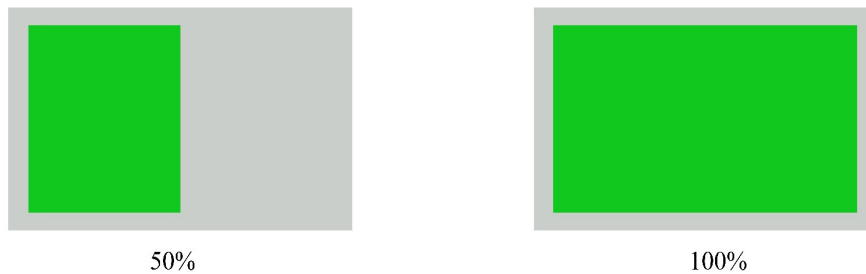


Figure 6. The plan of 50% and 100% green roof.

3. Results

The results of the study focus on three hours, which are 8:00, 14:00, and 20:00. The main reason is that 8:00 is usually the morning rush hour for daily commuting, while the summer temperature reaches the highest at 14:00. Meanwhile, the urban heat island effect is obvious during the first 2–3 h after the sun sets [60]; therefore, 20:00 is the chosen hour in the evening. In the following, the air temperature refers to the average value of nine receivers (Figure 2).

3.1. Baseline Scenario

It can be seen from Figure 7 that during the morning of 8:00–10:00, the temperature of LCZ-4 appears to be the highest, while LCZ-5 and LCZ-6 are slightly lower. The three types of LCZ all reach their peaks at 14:00. During the high temperature hours (12:00–14:00), the average air temperature of LCZ-6 reaches the highest T_a , and the LCZ-5 air temperature remains the lowest. After reaching the peak temperature, there is a downward trend in the air temperature for all three LCZs until 22:00–23:00. During the nighttime (20:00 to 5:00), the air temperature of LCZ-4, LCZ-5, and LCZ-6 are substantially coincident.

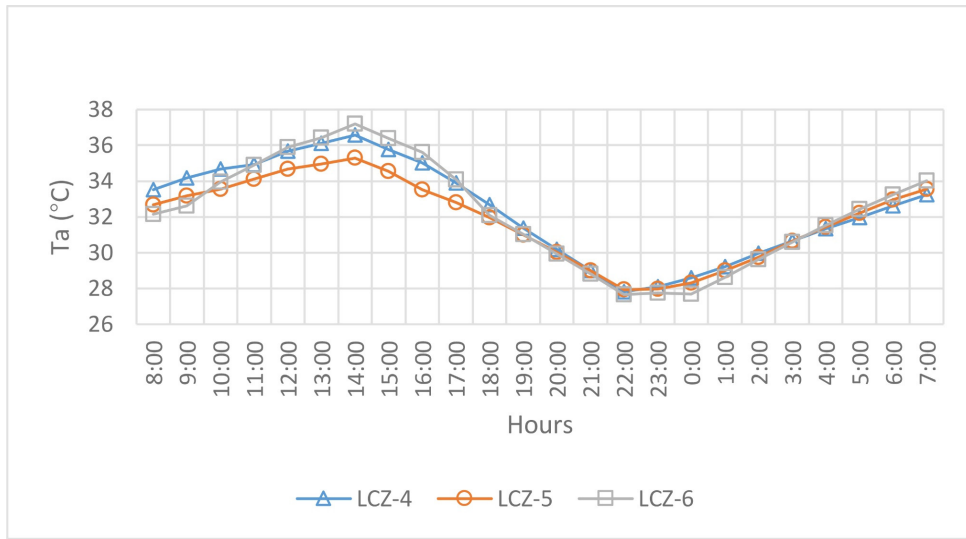


Figure 7. Average air temperature of nine receptors in LCZ-4, LCZ-5, and LCZ-6 in the Baseline scenario.

Figure 8 shows the air temperature distribution of the Baseline scenario at the selected three hours (8:00, 14:00, and 20:00). At 14:00, the northwest parts of LCZ-4 are cooler than the rest of the areas due to geometrical shading of streets by buildings. In LCZ-4, the street areas between buildings and the open areas in the southeast have higher temperatures, which can be explained by the low ground albedo materials and the lack of greenery within those areas. The low Ta areas of LCZ-5 (open middle-rise) are mainly concentrated in interspaced areas between buildings on the east. In contrast, the Ta layout of LCZ-6 at 14:00 indicates the asphalt has higher temperature compared with other pavement materials, mainly because the low buildings in LCZ-6 cannot create large areas of shadows, causing the air temperature increase at 14:00.

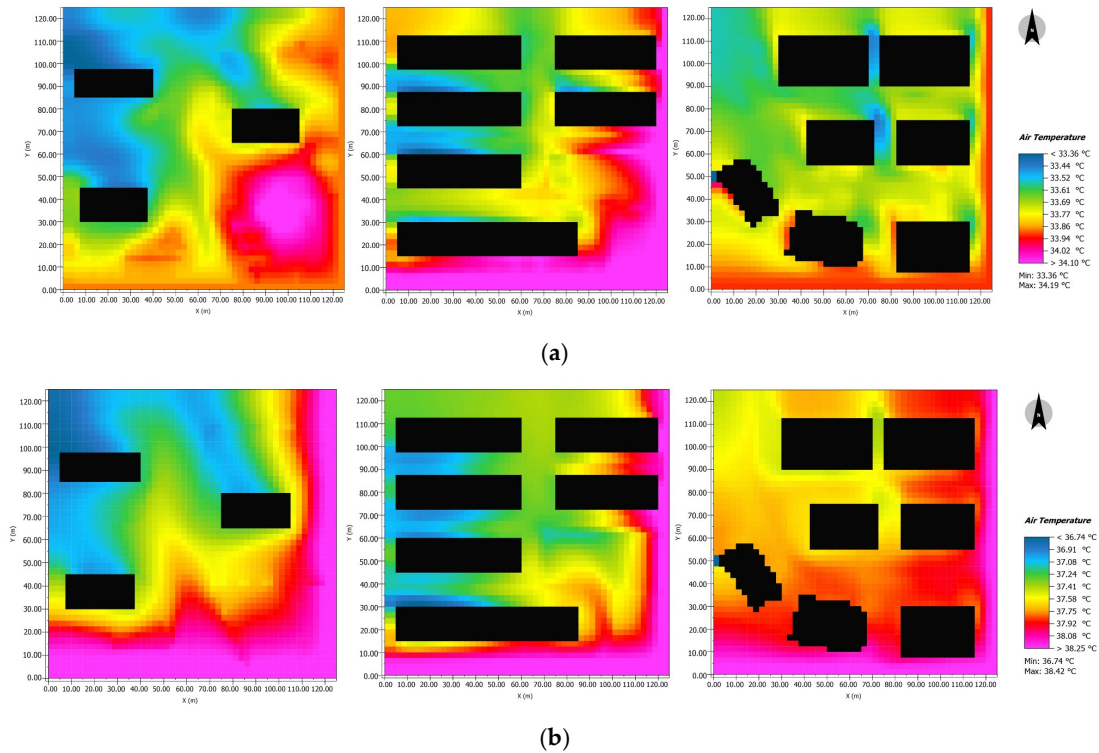


Figure 8. Cont.

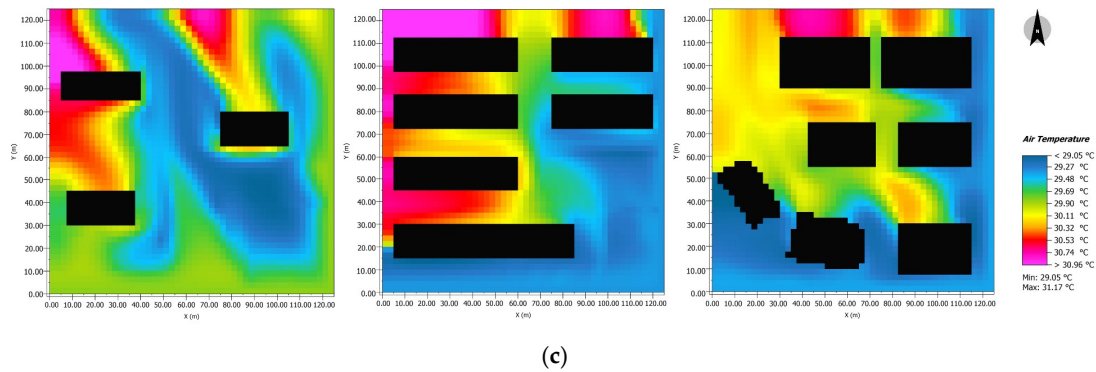


Figure 8. (a) Air temperature distribution of Baseline scenario in LCZ-4, LCZ-5, and LCZ-6 at 8:00; (b) Air temperature distribution of Baseline scenario in LCZ-4, LCZ-5, and LCZ-6 at 14:00; (c) Air temperature distribution of Baseline scenario in LCZ-4, LCZ-5, and LCZ-6 at 20:00.

3.2. Single Variable

3.2.1. Tree Quantity

All LCZs’ Ta values are reduced after the addition of trees. A 30% increase of tree covers (Scenario A) is sufficient to cut the incoming solar radiation and reduce average air temperature by 0.10–0.30 °C, while the 60% increase (Scenario B) shows an approximate drop of 0.10–0.60 °C during the day, indicating that more trees provide more effective cooling. However, the temperature drop is insignificant (0.08–0.18 °C) for every 30% tree increase by 20:00. This may due to an increase in tree block long wave radiation escaping to the night sky, which prevents the function of nocturnal cooling [75].

According to Figure 9, the greatest reductions are achieved along the street in LCZ-4, LCZ-5, and LCZ-6. LCZ-4 and LCZ-5 have relatively tall buildings, which are already well-shaded most of the day, which causes the increased tree quantity to be less effective. It is noted in Figure 9 that the Ta reduction around buildings is lower than in other areas because these zones are already cooler than the street area in the Baseline scenario due to geometrical shading by buildings. In LCZ-4, even though trees that are along the streets keep an obvious cooling effect at the peak hour 14:00 (Figure 9a), the impact is not significant enough to reduce the temperature of the entire site, especially in the areas that are not covered by tree shade and building shadows. For example, the temperature at measurement point #9 increases by 0.06 °C at 14:00, which is attributed to the direct exposure to sunlight, and thereby increases the evaporation of water in the soil. Likely, the prediction in LCZ-6 reveals a very similar Ta distribution, with larger Ta reduction along the street (marked by the red color in Figure 9c), because the trees could shade the street by intercepting the solar radiation as well as cooling the air by evapotranspiration, which results in relatively low temperatures for LCZ-6.

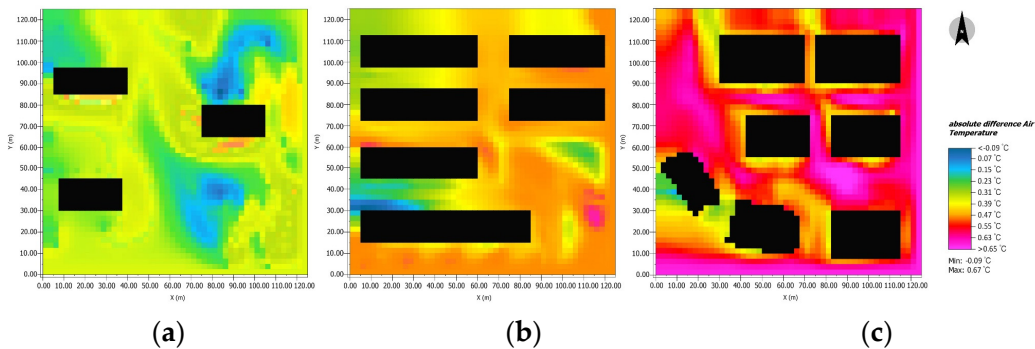


Figure 9. The Ta distribution of Baseline minus Scenario B in (a) LCZ-4, (b) LCZ-5, and (c) LCZ-6 at 14:00.

3.2.2. Green Roof

Comparing and contrasting among Baseline scenarios, Scenario C (50% green roof) and Scenario D (100% green roof) adding 100% green roof coverage had some cooling effect in certain regions for LCZ-6, mainly along the southeast wind direction (Figure 10). However, the air temperature reduction for LCZ-4 and LCZ-5 was insignificant. Additionally, the T_a reduction caused by 50% green roof was not obvious in all three LCZ classes. This result is consistent with the conclusion that as the building height increases, the microclimate impact of the green roof at pedestrian level decreases [76].

Figure 10 indicates that the elevation air temperature difference between Scenario D and the Baseline scenario in LCZ-6. The vertical average temperature drop is $0.09\text{ }^\circ\text{C}$ within four meters below the green roof. As the vertical height decreases, the air temperature reduction also drops. The air temperature reduction at the pedestrian height is only $0.04\text{ }^\circ\text{C}$ (Figure 10b).

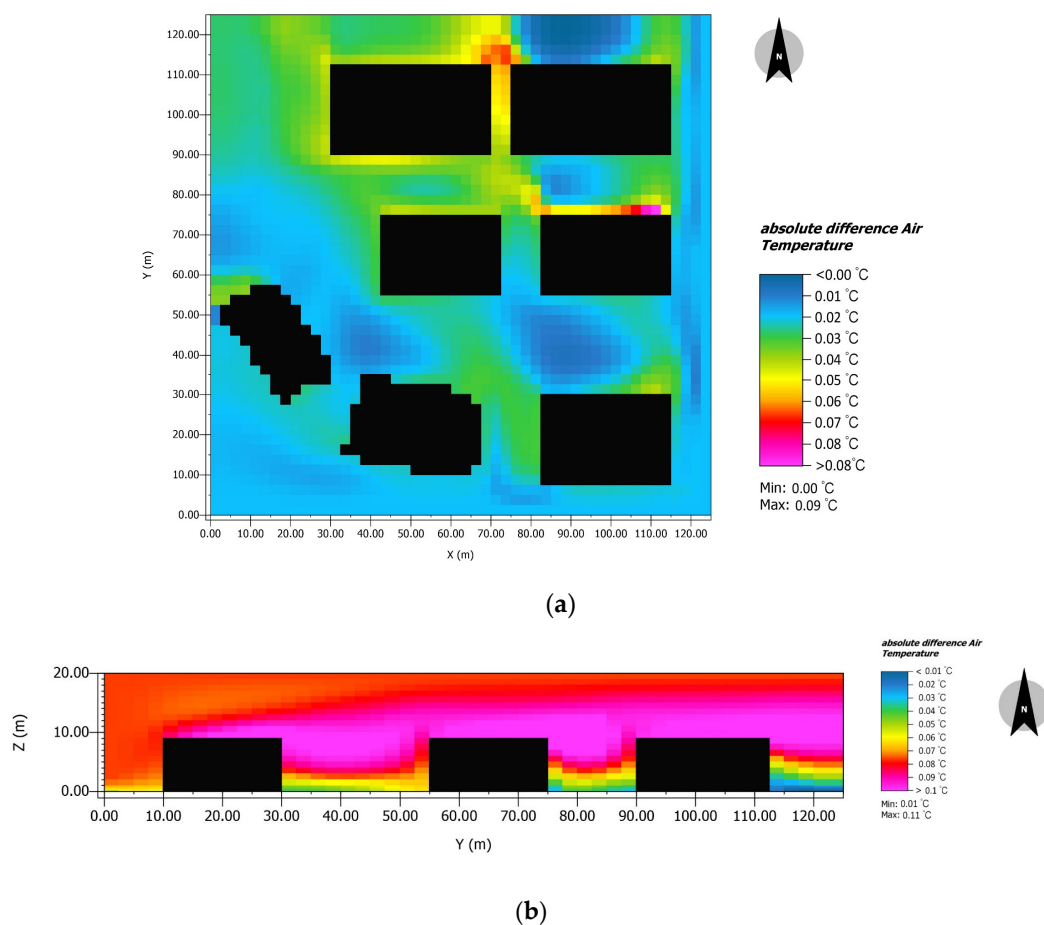


Figure 10. (a) T_a difference of Scenario D and Baseline scenario in LCZ-6 at 14:00; (b) Vertical ΔT_a at 14:00.

3.2.3. Ground Albedo

In Scenario E and Scenario F, the ground albedo was increased from 0.1 to 0.3 and 0.5, respectively. As can be observed in Table 5, the maximum T_a reduction of Scenario E is $0.12\text{--}0.49\text{ }^\circ\text{C}$ during the day. Although the cooling effect in Scenario F is more significant than that in Scenario E ($0.20\text{--}0.68\text{ }^\circ\text{C}$), similar T_a distributions are observed in LCZ-4, LCZ-5, and LCZ-6 (Figure 11).

Compared to the Baseline scenario at 14:00 (Figure 11), the T_a reduction of Scenario E and Scenario F in three LCZs is comparatively larger in the hard-paved area, while the air temperature drops in other areas are smaller. Specifically, it can be seen that the 0.20 albedo increase case exhibits temperatures up to $0.31\text{ }^\circ\text{C}$ lower in the road between buildings and up to an average of $0.25\text{ }^\circ\text{C}$ lower in southeast open

areas in LCZ-5 (Figure 11a). Higher albedo (an increase of 0.40) results in decrease of up to 0.53 °C in the main road and an average of 0.37 °C in the surrounding open area (Figure 11a) in LCZ-4.

Table 5. The average air temperature reductions of nine receptors influenced by the variation of albedo (ground material) at pedestrian height (2 m).

Albedo values	LCZ-4		LCZ-5		LCZ-6	
	+0.2	+0.4	+0.2	+0.4	+0.2	+0.4
8:00	−0.14	−0.21	−0.12	−0.23	−0.18	−0.20
14:00	−0.49	−0.68	−0.25	−0.49	−0.20	−0.38
20:00	−0.16	−0.15	−0.05	−0.10	−0.06	−0.16

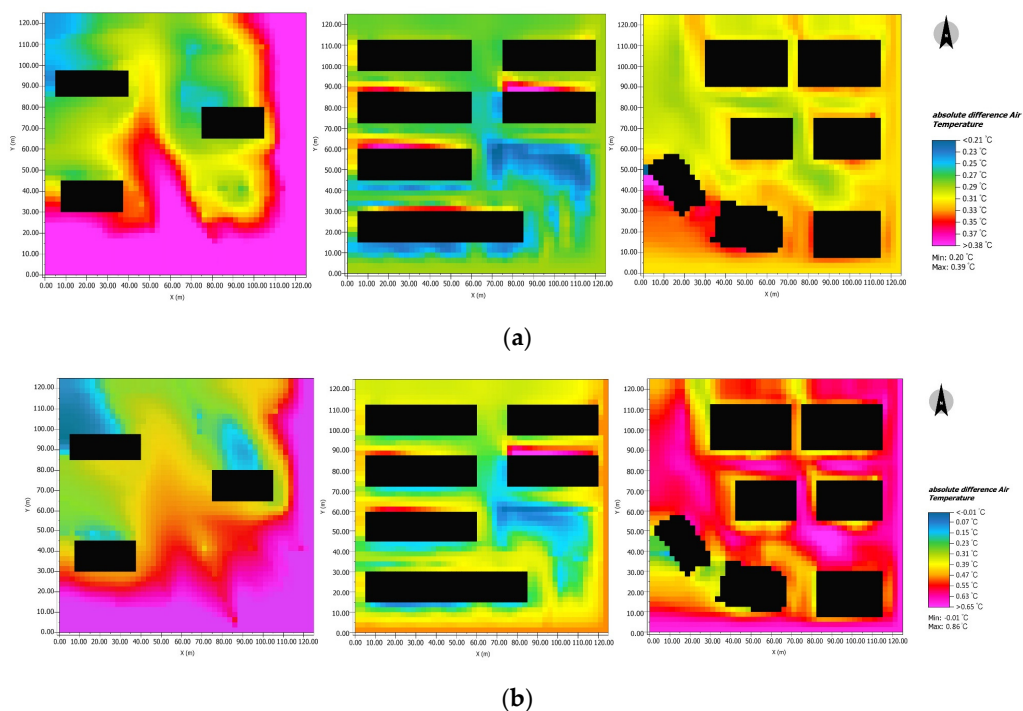


Figure 11. (a) The Ta difference between Baseline scenario and Scenario E in LCZ-4, LCZ-5, and LCZ-6 at 14:00; (b) The Ta difference between Baseline scenario and Scenario F in LCZ-4, LCZ-5, and LCZ-6 at 14:00.

Overall, the air temperature reduction in LCZ-4 is larger than that of LCZ-5 and LCZ-6 at 8:00 and 14:00 with higher albedo (Table 5). The air temperature reduction reaches a peak at 14:00, while it becomes negligible at 20:00 in all LCZs. The reason may be due to the ground materials with higher albedo cutting down ground surface temperature and promoting favorable evapotranspiration processes during the day.

From the simulation results we can see that the tree quantities and albedo have a negative correlation with air temperature, which confirms the cooling effect on pedestrian air temperature modification. However, the temperature drops of green roofs remain within 0.10 °C, even at 14:00 when the solar radiation is strong. Additionally, the cooling effects related to green roofs are not obvious regardless of whether 50% or 100% green roofs are covered, according to the linear regression in Figure 12c.

As can be observed in Figure 12, there is nearly a 0.14–0.40 °C reduction in air temperature per 30% increase in tree quantity and an approximate 0.10–0.50 °C decrease for every 0.20 increase in albedo at 14:00. Specifically, the slopes of the relationships are different depending on the LCZ classes. For LCZ-4, the cooling effect of increasing albedo outperforms the tree quantities and green roofs at

8:00 and 14:00. The decline in cooling capacity provided by increasing albedo 0.20 (from 0.40 °C reduce to less than 0.15 °C) is larger than that of increasing tree quantity. On the contrary, the cooling effect of albedo is better than tree quantities for LCZ-5 and LCZ-6 at 8:00 and 14:00.

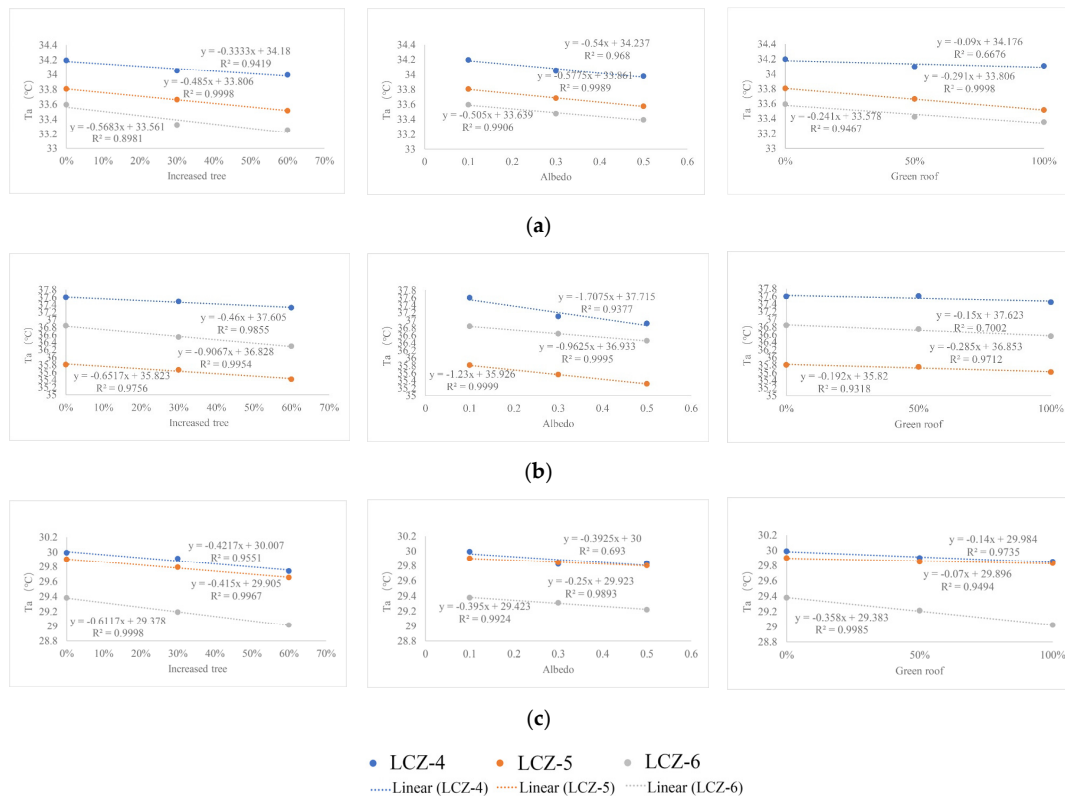


Figure 12. (a) Correlation between average air temperature and tree quantities, albedo, and green roof at 8:00; (b) Correlation between average air temperature and tree quantities, albedo, and green roof at 14:00; (c) Correlation between average air temperature and tree quantities, albedo, and green roof at 20:00.

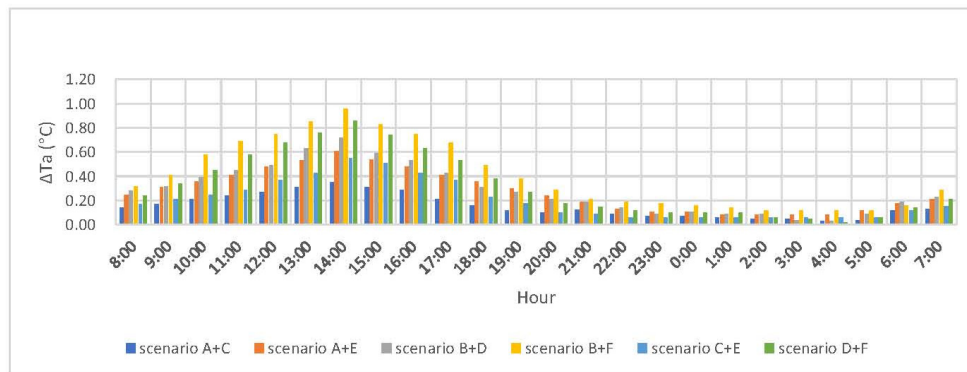
3.3. Two Variables

To further investigate the cooling method combinations, six different scenarios were simulated for LCZ-4-6. The 24-hour air temperature reduction is shown for the integrated scenarios in Figure 13. Comparing among Scenario A+C, Scenario A+E, Scenario B+D, Scenario B+F, Scenario C+E, and Scenario D+F, the air temperatures of the scenarios adopted with two variables are always lower than that in the Baseline scenario. Overall, the ΔT_{a-max} during 24 h occurs at 14:00 in the afternoon, and the ΔT_{a-min} during 24 h occurs during 1:00 to 4:00 in the morning for all the simulated scenarios. Moreover, two-variable scenarios have a more significant average cooling effect (reduction range from 0.02 to 0.96 °C) in LCZ-4, LCZ-5, and LCZ-6 compared to one-variable scenarios during the day (from 7:00 to 18:00). At nighttime (from 19:00 to 6:00), the temperature reductions of all scenarios are much less.

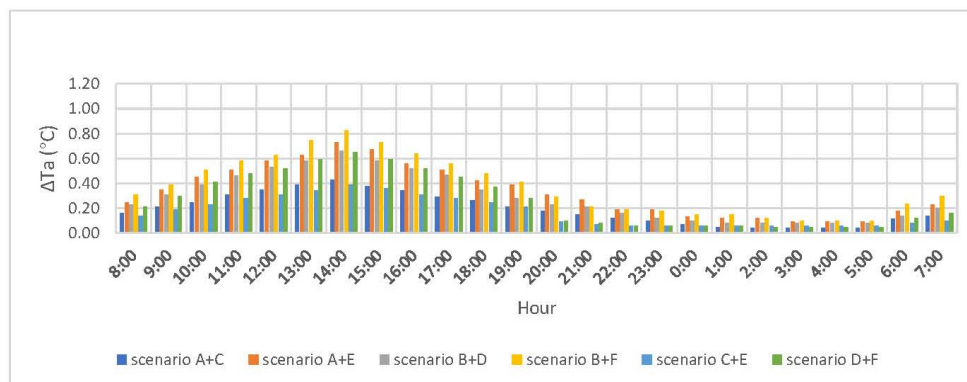
According to the previous single-variable simulation results, within the whole 24 h periods, the highest reduction of air temperature is originally obtained from large tree quantities combined with ground albedo. Even though less of an effect is found from the changes of green roof, it is easily believed that the two-variables combination has cooling potential, especially when tree quantities and higher ground albedo are integrated.

In fact, the combined-variable scenarios have a more significant cooling effect. For instance, Scenario A+E (increasing trees by 30%, increasing albedo by 0.2) provides higher reduction (0.96 °C), when compared to Scenario A (0.32 °C) and Scenario E (0.41 °C) in LCZ-4 at 14:00. Additionally, for the

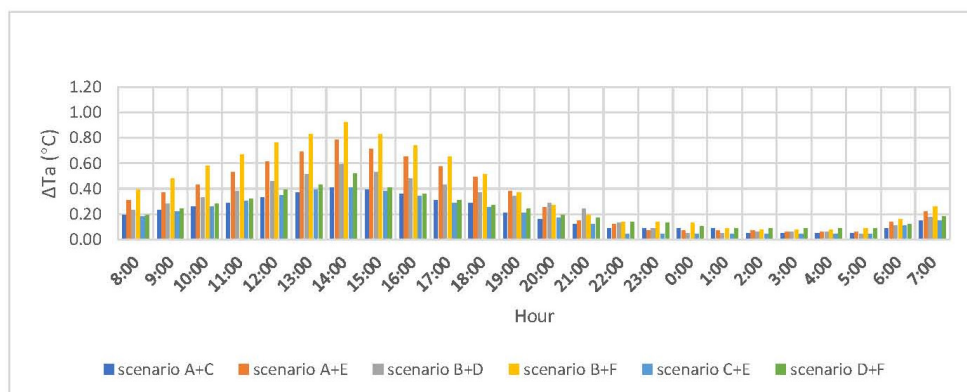
value of two-variable doubles (compare Scenario A+E and Scenario B+F), temperature reduction is also enhanced during the day. Particularly, Scenario B+F has the most significant air temperature reduction (0.30–0.96 °C) during the daytime. At the peak hour (14:00), the air temperature differences between Baseline scenario and Scenario B+F for LCZ-4, LCZ-5, and LCZ-6 are 0.96 °C, 0.83 °C, and 0.9 °C, respectively (Figure 13), which is attributed to the modification of ground materials, which could enhance the cooling effect of vegetation, with the low absorption of solar radiation and high ground surface moisture contents during the daytime.



(a)



(b)



(c)

Figure 13. Temperature reduction (°C) of 24 h from 08/01 8:00 to 08/02 8:00 compared with Baseline scenario at 2 m for six scenarios in (a) LCZ-4, (b) LCZ-5, and (c) LCZ-6.

In addition, cooling method combinations can provide more advantageous cooling effects when applied in the appropriate LCZ. This makes a maximum average difference with magnitude up to 0.35 °C. High Ta reduction of up to 0.55 °C (in LCZ-4) can be observed when applying Scenario C+F owing to the relatively high reflection of hard paving surfaces, while LCZ-6 appears to have a decrease of 0.40 °C with Scenario C+F at 14:00. Accordingly, the combined implementation Scenario D+F is found to lead to the larger reduction of air temperature in LCZ-4 (0.85 °C), while it only causes 0.50 °C in LCZ-6. The results of Scenario A+E also vary in different LCZs, with a Ta decrease of 0.60 °C, 0.71 °C, and 0.78 °C for LCZ-4, LCZ-5, and LCZ-6, respectively. This is because the trees in the low-rise open areas (LCZ-6) are not well-shaded by buildings, reducing Ta more than the other two LCZs during the hottest period of the day.

Specifically, comparing the six simulated double-variable scenarios in LCZ-4 (open high-rise model), the rate of reductions in temperatures tend to decline during the day. Scenario A+C (an increase of tree quantities by 30% and green roof by 50%) has the lowest ΔT_a (0.13–0.43 °C), while Scenario B+F (an increase of tree quantities by 60% and albedo by 0.4) has the highest ΔT_a (0.26–0.96 °C) during the day. However, during 0:00–5:00, Scenario A+C, Scenario A+E, Scenario B+D, and Scenario B+F have slight Ta reductions compared to the Baseline scenario in LCZ-4.

Likewise, the results exhibit a similar trend in LCZ-5 and LCZ-6, where the magnitude of daytime Ta is cooler than the Baseline scenarios. Scenario A+E and Scenario B+F are found to have corresponding Ta reduction ranges of 0.25 to 0.73 °C and 0.30 to 0.82 °C in LCZ-5, respectively. Then again, for LCZ-6, the Ta reduced by 0.30–0.80 °C and 0.40–0.92 °C in Scenario A+E and Scenario B+F, which is attributed to the increased tree number and higher ground albedo.

Furthermore, it is noticeable that air temperature differences exist among all the scenarios. Comparing Scenario B+F (increasing trees by 60%, increasing albedo by 0.4) with Scenario D+F (green roof 100%, increasing albedo by 0.4) at 14:00, even though they both have albedo increased by 0.4, the cooling effect of Scenario B+F is higher than that in Scenario D+F during the day, and the difference is most significant in LCZ-6 (0.20–0.40 °C). On the one hand, it again demonstrates that tree quantities contribute more cooling than green roofs. On the other hand, it shows that the cooling effect mostly comes from adding trees in LCZ-6, because shading is found to be an effective measure to mitigate high Ta in the low building area, which lacks building shadows. However, when comparing Scenario B+D (increasing trees by 60%, green roof 100%) with Scenario D+F (green roof 100%, increasing albedo by 0.4), Scenario B+D has higher air temperature than that of Scenario D+F in LCZ-4; however, they are nearly equal in LCZ-5. In LCZ-6, Scenario B+D shows lower Ta than that of Scenario D+F, which means in LCZ-4, the heat dissipation potential is obtained through the modification of the ground material in the combination variable outweigh trees, while it seems the opposite in LCZ-6. The contribution rate of the two is equivalent for LCZ-5.

In general, all the modifications are effective in reducing the air temperature in LCZ-4, LCZ-5, and LCZ-6. This verifies the hypothesis that the urban air temperature conditions reduce as tree quantity, ground surface albedo values, and green roof area increase. The appropriate cooling method combination should also be applied when considering the maximum cooling effect. During the peak hour (14:00) the combined modification of trees and ground albedo created a more advantageous effect of air temperature reduction in LCZ-4–6. Furthermore, it can be noticed that the two-variable scenarios with the increase of trees produced a noticeable cooling effect and kept the area cooler during the peak hour in LCZ-5 and LCZ-6.

4. Discussion

The outputs of single-variable simulations show that tree quantities provide notable temperature reduction in LCZ-4, LCZ-5, and LCZ-6. The result agrees with some previous research results, which show that increasing tree coverage in open and bare urban areas can effectively mitigate thermal conditions significantly [77,78]. Comparing between Scenario A and Scenario B, it can be found that adding 60% more trees outweighs a 30% increase during the selected three hours. Moreover, while

with the same vegetation coverage, LCZ-6 has the most significant decrease effect at 14:00. This may be due to the fact that adding trees could provide more shadows to cool down the human-height air temperature of the Baseline scenario in LCZ-6, which has the highest air temperature among all three LCZs. Especially during the hottest hour, tree covers have significant impacts on cutting down solar radiation for LCZ-6.

Furthermore, the temperature reductions caused by adding trees are slightly greater than those for the high albedo modification cases. During the peak hour (14:00), the average temperature decreases 0.20–0.50 °C every 0.2 increase in ground albedo, which agrees with the previous research that the relatively low albedo cause more thermal energy storage in pavement and tends to generate a more severe UHI effect [79], while the higher albedo surfaces in these conditions are likely to reflect solar radiation quickly and store only a negligible amount [43].

As shown in Figure 12, there is a negative linear relationship between the number of trees and air temperature. Similar conclusions were also reached in some of the previous studies. For example, tree canopy coverage is negatively associated with air temperature in Phoenix and Changchun [17,80]; however, the cooling capacity of the same number of trees is quite different, due to the distinct arrangement [17,70], location [81], tree species [28,32], and climate background [17]. On the contrary, the study in Prague and Brno suggests that adding trees (a 30% increase) in the compact midrise development might even increase air temperature [82]. This may be explained by the fact that the cooling effect of urban greenery differs with the surrounding urban structure, which again reveals the importance of UHI study under the LCZ framework. Furthermore, higher ground albedo leads to a decrease of air temperature, which agrees with previous studies. When the albedo of road increased from 0.2 to 0.45, the daily-averaged urban heat island intensity of the urban area decreased by about 0.1 °C in Montreal [83]. Similarly, in Rome, a higher improvement of urban temperature is noticed during the daytime where temperature is decreased by 4 °C if the albedo of surfaces increases [84]. The model in Prague and Brno suggests that an albedo increased by 0.25 leads to a difference of −0.2 °C in daily average temperature, while an albedo increased by 0.5 leads to a daily average temperature difference of −0.5 °C in Prague and −0.4 °C in Brno [82], which also proves the negative linear relationship between the albedo and air temperature. Even though these results vary in spatial scales, the cooling capability of higher albedo cannot be ignored.

Among the three individual cooling measures, the green roofs have the least noticeable cooling effect on the thermal environment at outdoor pedestrian height, especially for open high-rise and open middle-rise residential context (LCZ-4 and LCZ-5). A previous study shows that the green roof strategy can effectively reduce the temperature of the outer surface of the roof and help reduce the building energy consumption [85]. However, the cooling impacts of the green roofs on sidewalks at pedestrian height depend on the building height [86,87]. Furthermore, no obvious linear relationship is observed between 50% and 100% of green roofs in the three LCZs. It is noticeable that the T_a drop of green roof on the pedestrian height in this study is quite insignificant compared to the very few relevant studies [87]. The reason may be attributed to the improper physical characteristics of the green roof setting in the simulation, such as leaf area index, plant height, and soil thickness [88]. Additionally, the low percentage of green roof of each site may also contribute to insignificant T_a reduction [89].

Comparing one-variable with two-variable scenarios, firstly, given the same percentage, two-variable scenarios are superior to one-variable scenarios in cooling air temperature. Secondly, sometimes single cooling methods with high value can also achieve the same effect as cooling method combinations. For instance, Scenario B (increasing trees by 60%) has higher T_a reduction (0.41–0.67 °C) than Scenario A+C (increasing trees by 30% and albedo by 0.2) (ΔT_a 0.35–0.43 °C). Thirdly, even the same combination method has a different level of cooling in terms of different LCZ types. By providing an appropriate number of trees and high albedo materials, an optimum cooling level can be achieved, offering a significant reduction in the air temperature among all the simulated scenarios. In fact, a number of previous studies suggest that surface properties (i.e., building height, height-to width ratio, and sky view factor) are important factors of microclimate. As a new classification system, LCZ is

a useful tool to quantify and generalize the variety of surface properties in urban areas and make comparisons between cities easily. From the discussions above, different LCZs have their favorable combinations of cooling methods. This finding agrees with some of the previous research. For instance, the study in Baghdad indicates that trees can cause a 4 K reduction of T_a in the medium density building area; however, there is nearly no influence in the high-density district [90]. Some studies also point out that trees are more effective in low urban density (high sky view factor) than in compact urban areas (low sky view factor) [91].

Limitations and Future Direction

Although the study simulates and compares 36 cooling scenarios with three current situations for LCZ-4, LCZ-5, and LCZ-6, there are still some practical limitations. Firstly, solar radiation is only generated by the assumed conditions in the model and the wind is constantly from one direction, which does not reveal the actual situation. Secondly, studies show that intensive green roofs have a better cooling effect than extensive green roofs [88,89,92]. However, the intensive green roof type is not considered as a variable in the simulation, which may lead to the result that there is a non-linear relationship between green roof and cooling effect. Further studies are needed in terms of considering leaf area index, plant height, and soil thickness as variables to explore the cooling effects of green roofs. The building's physical properties such as building layout, building surface fraction, and the number of buildings of the chosen sites may also lead to the limited area of green roof and unsatisfactory simulation results. Additionally, specific tree locations and arrangements are not taken into consideration in the research, which may have an influence on shading and ventilation [17], and the species is limited to *Cinnamomum camphor*, which is also one of the restricted settings. More studies are necessary to find the appropriate tree arrangements and species in terms of optimum cooling impact. Furthermore, each LCZ scenario was modelled in isolation without the surrounding environment; thus, the shading effects and ventilation between neighborhoods could not be taken into account. Lastly, the cooling methods may not be effective in another climate zone such as the tropical monsoon climate cities. Further discussions are needed in the rest of the LCZ classes and other cities of different climate zones.

5. Conclusions

The research aimed at exploring the cooling potential of tree quantity, ground albedo, green roofs and their combinations in LCZ-4, LCZ-5, and LCZ-6. Firstly, from the simulation results, it is demonstrated that all the cooling method scenarios have an influence on air temperature reduction, except for the extensive green roof index, which presents a negligible effect on air temperature at human height in all three LCZs regardless of its proportion. Even though 100% green roof modification affects pedestrian air temperature in low building areas (LCZ-6), the reduction of which is only 0.04 °C. In that case, the relationship between the cooling capacity and the green roof is not linear, whereas tree shade and higher albedo can provide effective local cooling.

Secondly, the contributory factor effects differ among different urban morphology types (LCZs). Increasing the quantity of trees by 60% leads to lower outdoor temperatures at pedestrian height for LCZ-5 and LCZ-6. However, due to the large but unshaded open space and inter-spacing between buildings, the effect of increasing trees by 30% or 60% is not as good as that in mid-rise and low-rise building areas, which makes some regions of LCZ-4 suffer from high air temperature. On the contrary, the effect of albedo modification on air temperature is likely to be valid in LCZ-4. Even though green roofs play the most insignificant role among three methods, they displays some T_a reduction in low buildings (LCZ-6). As they do not need to use valuable and highly competitive land at ground level, they can be used as a cooling method when the public space is limited in LCZ-6.

Thirdly, by applying combined cooling factors, a decrease in air temperature can be provoked in an open residential context (LCZ-4, LCZ-5 and LCZ-6), and especially with higher levels of tree quantity (60%) coupled with cool ground material (increased albedo of 0.4), the cooling effect is significantly

enhanced. The variations in the estimated benefits among 36 scenarios reflect the importance of cooling analysis aimed at different open LCZs.

In conclusion, vegetated scenarios in LCZ-5 and LCZ-6 enhance cooling effect, especially in the 60% more trees scenarios due to shade density, while higher albedo scenarios in LCZ-4 lead to a significant reduction. Therefore, when considering one cooling strategy, this study recommends adding 60% more trees in LCZ-5 and LCZ-6, while increasing albedo (by 0.4) in LCZ-4. Additionally, Scenario B+E (60% more trees and 0.4 higher ground albedo) is the most effective scenario in LCZ-4, LCZ-5, and LCZ-6 at pedestrian height. Thus, it is recommended that two major factors (trees and ground albedo) need to be considered in combination when planning and renewing open building areas, ultimately offering improvement in the thermal environment. Furthermore, it is not recommended to apply an extensive type of green roof in LCZ-4 and LCZ-5 when only considering decreasing air temperature at pedestrian height due to its negligible cooling effect. The findings obtained from this study should be extended to other LCZ types and climatic regions in future research.

Author Contributions: Conceptualization, Y.C.; methodology, Y.C.; formal analysis, Y.C.; investigation, Y.C. and Y.H.; writing—original draft preparation, Y.C.; writing—review and editing, Y.H.; supervision, B.Z.; funding acquisition, Y.C. and B.Z.; All authors have read and agreed to the published version of the manuscript.

Funding: This research was funded by National Nature Science Foundation of China, grant number 51608535, 31901363; Nature Science Foundation of Hunan Province, China, grant number 2019JJ50990; Fundamental Research Funds for the Central Universities, grant number 2018zzts091.

Conflicts of Interest: The authors declare no conflict of interest.

References

1. Hamdi, R.; Duchêne, F.; Berckmans, J. Evolution of urban heat wave intensity for the Brussels capital region in the ARPEGE-Climat A1B scenario. *Urban Clim.* **2016**, *17*, 176–195. [[CrossRef](#)]
2. European Environment Agency. *Urban Adaptation to Climate Change in Europe*; EEA Report 2/2012; © EEA: Copenhagen, Denmark, 2012; ISBN 978-92-9213-308-5, ISSN 1725–9177. [[CrossRef](#)]
3. Skarbit, N.; Stewart, I.D.; Unger, J. Employing an urban meteorological network to monitor air temperature conditions in the ‘local climate zones’ of Szeged, Hungary. *Int. J. Climatol.* **2017**, *37*, 582–596. [[CrossRef](#)]
4. Tan, J.; Zheng, Y.; Tang, X. The urban heat island and its impact on heat waves and human health in Shanghai. *Int. J. Biometeorol.* **2010**, *54*, 75–84. [[CrossRef](#)] [[PubMed](#)]
5. Fenner, D.; Meier, F.; Scherer, D. Spatial and temporal air temperature variability in Berlin, Germany, during the years 2001–2010. *Urban Clim.* **2014**, *10*, 308–331. [[CrossRef](#)]
6. Žuvela-Aloise, M.; Andre, K.; Schwaiger, H. Modelling reduction of urban heat load in Vienna by modifying surface properties of roofs. *Theor. Appl. Climatol.* **2018**, *131*, 1005–1018. [[CrossRef](#)]
7. Kovats, R.S.; Hajat, S. Heat stress and public health: A critical review. *Annu. Rev. Public Health* **2008**, *29*, 41–55. [[CrossRef](#)]
8. Savi, S.; Markovi, V.; Šecero, I. Heat wave risk assessment and mapping in urban areas: Case study for a midsized Central European city, Novi Sad (Serbia). *Nat. Hazard.* **2018**, *91*, 891–911. [[CrossRef](#)]
9. Miron, I.J.; Linares, C.; Montero, J.C. Changes in cause-specific mortality during heat waves in central Spain, 1975–2008. *Int. J. Biometeorol.* **2015**, *59*, 1213–1222. [[CrossRef](#)]
10. Son, J.Y.; Gouveia, N.; Bravo, M.A. The impact of temperature on mortality in a subtropical city: Effects of cold, heat, and heat waves in São Paulo, Brazil. *Int. J. Biometeorol.* **2016**, *60*, 113–121. [[CrossRef](#)]
11. Wang, Z.H.; Zhao, X.; Yang, J. Cooling and energy saving potentials of shade trees and urban lawns in a desert city. *Appl. Energy* **2016**, *161*, 437–444. [[CrossRef](#)]
12. Tsoka, S. Investigating the relationship between urban spaces morphology and local microclimate: A study for the Salonika. *Procedia Environ. Sci.* **2017**, *38*, 674–681. [[CrossRef](#)]
13. Denise, H.S.D.; Paula, S.; Carolina, D.S.G. The impact of vegetation on urban microclimate to counterbalance built density in a subtropical changing climate. *Urban Clim.* **2015**, *14*, 224–239.
14. Yang, X.; Li, Y. The impact of building density and building height heterogeneity on average urban albedo and street surface temperature. *Build. Environ.* **2015**, *90*, 146–156. [[CrossRef](#)]

15. Sharmin, T.; Steemers, K.; Matzarakis, A. Microclimatic modelling in assessing the impact of urban geometry on urban thermal environment. *Sustain. Cities Soc.* **2017**, *34*, 293–308. [[CrossRef](#)]
16. Giannopoulou, K.; Santamouris, M.; Livada, I. The impact of canyon geometry on intra urban and urban: Suburban night temperature differences under warm weather conditions. *Pure Appl. Geophys.* **2010**, *167*, 1433–1449. [[CrossRef](#)]
17. Wu, Z.; Dou, P.; Chen, L. Comparative and combinative cooling effects of different spatial arrangements of buildings and trees on microclimate. *Sustain. Cities Soc.* **2019**, *51*, 101711. [[CrossRef](#)]
18. Hwang, W.; Wiseman, P.E.; Thomas, V.A. Enhancing the energy conservation benefits of shade trees in dense residential developments using an alternative tree placement strategy. *Landsc. Urban Plan.* **2017**, *158*, 62–74. [[CrossRef](#)]
19. Peng, L.L.H.; Yang, X.; He, Y. Thermal and energy performance of two distinct green roofs: Temporal pattern and underlying factors in a subtropical climate. *Energy Build.* **2019**, *185*, 247–258. [[CrossRef](#)]
20. Wang, Y.; Ni, Z.; Chen, S. Microclimate regulation and energy saving potential from different urban green infrastructures in a subtropical city. *J. Clean. Prod.* **2019**, *226*, 913–927. [[CrossRef](#)]
21. Srivani, M.; Hokao, K. Evaluating the cooling effects of greening for improving the outdoor thermal environment at an institutional campus in the summer. *Build. Environ.* **2013**, *66*, 158–172. [[CrossRef](#)]
22. Imran, H.M.; Kala, J.; Ng, A.W.M. Effectiveness of vegetated patches as Green Infrastructure in mitigating Urban Heat Island effects during a heatwave event in the city of Melbourne. *Weather Clim. Extrem.* **2019**, *25*, 100217. [[CrossRef](#)]
23. Aboelat, A.; Sodoud, S. Evaluating the effect of trees on UHI mitigation and reduction of energy usage in different built up areas in Cairo. *Build. Environ.* **2020**, *168*, 106490. [[CrossRef](#)]
24. Xiao, X.D.; Dong, L.; Yan, H. The influence of the spatial characteristics of urban green space on the urban heat island effect in Suzhou Industrial Park. *Sustain. Cities Soc.* **2018**, *40*, 428–439. [[CrossRef](#)]
25. Tan, Z.; Lau, K.L.; Ng, E. Urban tree design approaches for mitigating daytime urban heat island effects in a high-density urban environment. *Energy Build.* **2016**, *114*, 265–274. [[CrossRef](#)]
26. Srivani, M.; Jareemit, D. Modeling the influences of layouts of residential townhouses and tree-planting patterns on outdoor thermal comfort in Bangkok suburb. *J. Build. Eng.* **2020**, *30*, 101262. [[CrossRef](#)]
27. Morakinyo, T.E.; Lau, K.K.; Ren, C. Performance of Hong Kong's common trees species for outdoor temperature regulation, thermal comfort and energy saving. *Build. Environ.* **2018**, *137*, 157–170. [[CrossRef](#)]
28. Abreu-Harbach, L.; Labaki, L.C.; Matzarakis, A. Effect of tree planting design and tree species on human thermal comfort in the tropics. *Landsc. Urban Plan.* **2015**, *138*, 99–109. [[CrossRef](#)]
29. Zheng, S.; Zhao, L.; Li, Q. Numerical simulation of the impact of different vegetation species on the outdoor thermal environment. *Urban For. Urban Green.* **2016**, *18*, 138–150. [[CrossRef](#)]
30. Feyisa, G.L.; Dons, K.; Meilby, H. Efficiency of parks in mitigating urban heat island effect: An example from Addis Ababa. *Landsc. Urban Plan.* **2014**, *123*, 87–95. [[CrossRef](#)]
31. Armson, D.; Stringer, P.; Ennos, A.R. The effect of tree shade and grass on surface and globe temperatures in an urban area. *Urban For. Urban Green.* **2012**, *11*, 245–255. [[CrossRef](#)]
32. Morakinyo, T.; Kong, L.; Lau, K. A study on the impact of shadow—Cast and tree species on in-canyon and neighbourhood's thermal comfort. *Build. Environ.* **2017**, *115*, 1–17. [[CrossRef](#)]
33. Shahidan, M.F.; Jones, P.J.; Gwilliam, J. An evaluation of outdoor and building environment cooling achieved through combination modification of trees with ground materials. *Build. Environ.* **2012**, *58*, 245–257. [[CrossRef](#)]
34. Sanchez, L.; Reames, T.G. Cooling Detroit: A socio-spatial analysis of equity in green roofs as an urban heat island mitigation strategy. *Urban For. Urban Green.* **2019**, *44*, 126331. [[CrossRef](#)]
35. Farhadia, H.; Faizi, M.; Sanaieian, H. Mitigating the urban heat island in a residential area in Tehran: Investigating the role of vegetation, materials, and orientation of buildings. *Sustain. Cities Soc.* **2019**, *46*, 101448. [[CrossRef](#)]
36. Ran, J.; Tang, M. Effect of Green Roofs Combined with Ventilation on Indoor Cooling and Energy Consumption. *Energy Procedia* **2017**, *141*, 260–266. [[CrossRef](#)]
37. Susca, T.; Gaffin, S.R.; Dell'Osso, G.R. Positive effects of vegetation: Urban heat island and green roofs. *Environ. Pollut.* **2011**, *159*, 2119–2126. [[CrossRef](#)]
38. Feitos, R.C.; Sara, J. Wilkinson Small-scale experiments of seasonal heat stress attenuation through a combination of green roof and green walls. *J. Clean. Prod.* **2020**, *250*, 119443. [[CrossRef](#)]

39. Bevilacqua, P.; Mazzeo, D.; Bruno, R. Surface temperature analysis of an extensive green roof for the mitigation of urban heat island in southern Mediterranean climate. *Energy Build.* **2017**, *150*, 318–327. [[CrossRef](#)]
40. Collins, S.; Kuoppamaki, K.; Kotze, D.J. Thermal behavior of green roofs under Nordic winter conditions. *Build. Environ.* **2017**, *122*, 206–214. [[CrossRef](#)]
41. Yang, J.; Kumar, D.M.; Pyrgoub, A. Green and cool roofs' urban heat island mitigation potential in tropical climate. *Sol. Energy* **2018**, *173*, 597–609. [[CrossRef](#)]
42. Azeña, V.; Cuxart, J.; Picos, R. Thermal regulation capacity of a green roof system in the Mediterranean region: The effects of vegetation and irrigation level. *Energy Build.* **2018**, *164*, 226–238. [[CrossRef](#)]
43. Chen, J.; Zhou, Z.; Wu, J. Field and laboratory measurement of albedo and heat transfer for pavement materials. *Constr. Build. Mater.* **2019**, *202*, 46–57. [[CrossRef](#)]
44. Falasca, S.; Ciancio, V.; Salata, F. High albedo materials to counteract heat waves in cities: An assessment of meteorology, buildings energy needs and pedestrian thermal comfort. *Build. Environ.* **2019**, *163*, 106242. [[CrossRef](#)]
45. Enríquez, E.; Fuertes, V.; Cabrera, M.J. New strategy to mitigate urban heat island effect: Energy saving by combining high albedo and low thermal diffusivity in glass ceramic materials. *Sol. Energy* **2017**, *149*, 114–124. [[CrossRef](#)]
46. Benrazavi, R.S.; Binti Dola, K.; Ujang, N. Effect of pavement materials on surface temperatures in tropical environment. *Sustain. Cities Soc.* **2016**, *22*, 94–103. [[CrossRef](#)]
47. Yuan, J.; Emura, K.; Farnham, C. Is urban albedo or urban green covering more effective for urban microclimate improvement? A simulation for Osaka. *Sustain. Cities Soc.* **2017**, *32*, 78–86. [[CrossRef](#)]
48. Qin, Y. A review on the development of cool pavements to mitigate urban heat island effect, *Renew. Sustain. Energy Rev.* **2015**, *52*, 445–459.
49. Taleghani, M.; Berardi, U. The effect of pavement characteristics on pedestrian's thermal comfort in Toronto. *Urban Clim.* **2018**, *24*, 449–459. [[CrossRef](#)]
50. Taleghani, M. The impact of increasing urban surface albedo on outdoor summer thermal comfort within a university campus. *Urban Clim.* **2018**, *24*, 175–184. [[CrossRef](#)]
51. Lan, Y.; Zhan, Q. How do urban buildings impact summer air temperature? The effects of building configurations in space and time. *Build. Environ.* **2017**, *125*, 88–98. [[CrossRef](#)]
52. Lima, I.; Scalco, V.; Lamberts, R. Estimating the impact of urban densification on high-rise office building cooling loads in a hot and humid climate. *Energy Build.* **2019**, *182*, 30–44. [[CrossRef](#)]
53. Shashua-Bar, L.; Hoffman, M.E. Quantitative evaluation of passive cooling of the UCL microclimate in hot regions in summer, case study: Urban streets and court yards with trees. *Build. Environ.* **2004**, *39*, 1087–1099. [[CrossRef](#)]
54. Stewart, I.D.; Oke, T.R. Local Climate Zones for Urban Temperature Studies. *Bull. Am. Meteorol. Soc.* **2012**, *93*, 1879–1900. [[CrossRef](#)]
55. Wang, R.; Cai, M.; Ren, C. Detecting multi-temporal land cover change and land surface temperature in Pearl River Delta by adopting local climate zone. *Urban Clim.* **2019**, *28*, 100455. [[CrossRef](#)]
56. Bokwa, A.; Geletič, J.; Lehnert, M. Heat load assessment in Central European cities using an urban climate model and observational monitoring data. *Energy Build.* **2019**, *201*, 53–69. [[CrossRef](#)]
57. Geletič, J.; Lehnert, M.; Savić, S. Inter-/intra-zonal seasonal variability of the surface urban heat island based on local climate zones in three central European cities. *Build. Environ.* **2019**, *156*, 21–32. [[CrossRef](#)]
58. Wang, R.; Cai, M.; Ren, C. Modelled spatiotemporal variability of outdoor thermal comfort in local climate zones of the city of Brno, Czech Republic. *Sci. Total Environ.* **2018**, *624*, 385–395.
59. Lehnert, M.; Geletič, J.; Dobrovolný, P. Temperature differences among local climate zones established by mobile measurements in two central European cities. *Clim. Res.* **2018**, *75*, 53–64. [[CrossRef](#)]
60. Leconte, F.; Bouyer, J.; Claverie, R. Using Local Climate Zone scheme for UHI assessment: Evaluation of the method using mobile measurements. *Build. Environ.* **2015**, *83*, 39–49. [[CrossRef](#)]
61. Middel, A.; Häbb, K.; Anthony, J. Impact of urban form and design on mid-afternoon microclimate in Phoenix Local Climate Zones. *Landsc. Urban Plan.* **2014**, *122*, 16–28. [[CrossRef](#)]
62. Aminipouria, M.; Raynerb, D.; Lindberg, F. Urban tree planting to maintain outdoor thermal comfort under climate change: The case of Vancouver's local climate zones. *Build. Environ.* **2019**, *158*, 226–236. [[CrossRef](#)]

63. National Meteorological Information Centre. Available online: <http://data.cma.cn/> (accessed on 1 June 2019).
64. Hunan Meteorological Bureau, China. Available online: <http://hn.cma.gov.cn/> (accessed on 23 September 2019).
65. Ministry of Housing and Urban-Rural Development of the People's Republic of China. *Code for Thermal Design of Civil Building (GB 50176-2016)*, 1st ed.; China Construction Industry Press: Beijing, China, 2016; pp. 27–28.
66. Chen, Z. On the Influence of Greening System on the Outdoor Thermal Environment of Building Groups in Hot and Humid Areas. Ph.D. Thesis, South China University of Technology, Guangzhou, China, 2010.
67. López-Cabeza, V.P.; Galán-Marín, C.; Rivera-Gómez, C. Courtyard microclimate ENVI-met outputs deviation from the experimental data. *Build. Environ.* **2018**, *144*, 129–141. [[CrossRef](#)]
68. Acero, J.A.; Herranz-Pascual, K. A comparison of thermal comfort conditions in four urban spaces by means of measurements and modelling techniques. *Build. Environ.* **2015**, *93*, 245–257. [[CrossRef](#)]
69. Tsoka, S.; Tsikaloudaki, A.; Theodosiou, T. Analyzing the ENVI-met microclimate model's performance and assessing cool materials and urban vegetation applications—A review. *Sustain. Cities Soc.* **2018**, *43*, 55–76. [[CrossRef](#)]
70. Myint, S.W.; Zheng, B.; Talen, E. Does the spatial arrangement of urban landscape matter? Examples of urban warming and cooling in Phoenix and Las Vegas. *Ecosyst. Health Sustain.* **2015**, *1*, 1–15. [[CrossRef](#)]
71. Kolokotsa, D.; Santamouris, M.; Zerefos, S.C. Green and cool roofs' urban heat island mitigation potential in European climates for office buildings under free floating conditions. *Sol. Energy* **2013**, *95*, 118–130. [[CrossRef](#)]
72. Carter, T.; Keeler, A. Life-cycle cost–benefit analysis of extensive vegetated roof systems. *J. Environ. Manag.* **2008**, *87*, 350–363. [[CrossRef](#)]
73. Heidarinejad, G.; Esmaili, A. Numerical simulation of the dual effect of green roof thermal performance. *Energy Convers. Manag.* **2015**, *106*, 1418–1425. [[CrossRef](#)]
74. Santamouris, M. Using cool pavements as a mitigation strategy to fight urban heat island—A review of the actual developments. *Renew. Sustain. Energy Rev.* **2013**, *26*, 224–240. [[CrossRef](#)]
75. Upreti, R.; Wang, Z.; Yang, J. Radiative shading effect of urban trees on cooling the regional built environment. *Urban For. Urban Green.* **2017**, *26*, 18–24. [[CrossRef](#)]
76. Berardi, U. The outdoor microclimate benefits and energy saving resulting from green roofs retrofits. *Energy Build.* **2016**, *121*, 217–229.
77. Tan, Z.; Lau, K.; Ng, E. Planning strategies for road side tree planting and outdoor 541 comfort enhancement in subtropical high—Density urban areas. *Build. Environ.* **2017**, *120*, 93–109. [[CrossRef](#)]
78. Sodoudi, S.; Zhang, H.; Chi, X. The influence of spatial configuration of green areas on microclimate and thermal comfort. *Urban For. Urban Green.* **2018**, *34*, 85–96. [[CrossRef](#)]
79. Kyriakodis, G.E.; Santamouris, M. Using reflective pavements to mitigate urban heat island in warm climates—Results from a large scale urban mitigation project. *Urban Clim.* **2018**, *24*, 326–339. [[CrossRef](#)]
80. Middel, A.; Chhetri, N.; Quay, R. Urban forestry and cool roofs: Assessment of heat mitigation strategies in Phoenix residential neighborhoods. *Urban For. Urban Green.* **2014**, *14*, 178–186.
81. Zhao, Q.; Sailor, D.J.; Wentz, E.A. Impact of tree locations and arrangements on outdoor microclimates and human thermal comfort in an urban residential environment. *Urban For. Urban Green.* **2018**, *32*, 81–91. [[CrossRef](#)]
82. Geletič, J.; Lehnert, M.; Jurek, M. Spatiotemporal variability of air temperature during a heat wave in real and modified landcover conditions: Prague and Brno (Czech Republic). *Urban Clim.* **2020**, *31*, 100588. [[CrossRef](#)]
83. Touchaei, A.G.; Akbari, H. Evaluation of the seasonal effect of increasing albedo on urban climate and energy consumption of buildings in Montreal. *Urban Clim.* **2015**, *14*, 278–289. [[CrossRef](#)]
84. Morini, E.; Touchaei, A.G.; Rossia, F. Evaluation of albedo enhancement to mitigate impacts of urban heat island in Rome (Italy) using WRF meteorological model. *Urban Clim.* **2018**, *24*, 551–566. [[CrossRef](#)]
85. Kolokotsa, D.; Giannariakis, G.; Gobakis, K. Cool roofs and cool pavements application in Acharnes, Greece. *Sustain. Cities Soc.* **2018**, *37*, 466–474. [[CrossRef](#)]
86. Taleghani, M.; Sailor, D.; Ban-Weiss, G.A. Micrometeorological simulations to predict the impacts of heat mitigation strategies on pedestrian thermal comfort in a Los Angeles neighborhood. *Environ. Res. Lett.* **2016**, *11*, 024003. [[CrossRef](#)]
87. Jin, C.Q.; Bai, X.L.; Luo, T. Effects of green roofs' variations on the regional thermal environment using measurements and simulations in Chongqing, China. *Urban For. Urban Green.* **2018**, *29*, 223–237. [[CrossRef](#)]

88. Zeng, C.; Bai, X.; Sun, L. Optimal parameters of green roofs in representative cities of four climate zones in China: A simulation study. *Energy Build.* **2017**, *150*, 118–131. [[CrossRef](#)]
89. Susca, T. Green roofs to reduce building energy use? A review on key structural factors of green roofs and their effects on urban climate. *Build. Environ.* **2019**, *162*, 106273. [[CrossRef](#)]
90. Karlessi, T.; Santamouris, M.; Apostolakis, K. Development and testing of thermochromics coatings for buildings and urban structures. *Sol. Energy* **2009**, *83*, 538–551. [[CrossRef](#)]
91. Li, H.; Harvey, J.T.; Holland, T.J. The use of reflective and permeable pavements as a potential practice for heat island mitigation and storm water management. *Environ. Res. Lett.* **2013**, *8*, 15–23.
92. Yin, H.W.; Kong, F.H.; Dronova, I. Investigation of extensive green roof outdoor spatio-temporal thermal performance during summer in a subtropical monsoon climate. *Sci. Total Environ.* **2019**, *696*, 133976. [[CrossRef](#)]



© 2020 by the authors. Licensee MDPI, Basel, Switzerland. This article is an open access article distributed under the terms and conditions of the Creative Commons Attribution (CC BY) license (<http://creativecommons.org/licenses/by/4.0/>).